

We are IntechOpen, the world's leading publisher of Open Access books Built by scientists, for scientists

4,800

Open access books available

122,000

International authors and editors

135M

Downloads

Our authors are among the

154

Countries delivered to

TOP 1%

most cited scientists

12.2%

Contributors from top 500 universities



WEB OF SCIENCE™

Selection of our books indexed in the Book Citation Index
in Web of Science™ Core Collection (BKCI)

Interested in publishing with us?
Contact book.department@intechopen.com

Numbers displayed above are based on latest data collected.
For more information visit www.intechopen.com



Wireless Power Transfer for Miniature Implantable Biomedical Devices

Qi Xu, Tianfeng Wang, Shitong Mao, Wenyan Jia, Zhi-Hong Mao and Mingui Sun

Abstract

Miniature implantable electronic devices play increasing roles in modern medicine. In order to implement these devices successfully, the wireless power transfer (WPT) technology is often utilized because it provides an alternative to the battery as the energy source; reduces the size of implant substantially; allows the implant to be placed in a restricted space within the body; reduces both medical cost and chances of complications; and eliminates repeated surgeries for battery replacements. In this work, we present our recent studies on WPT for miniature implants. First, a new implantable coil with a double helix winding is developed which adapts to tubularly shaped organs within the human body, such as blood vessels and nerves. This coil can be made in the planar form and then wrapped around the tubular organ, greatly simplifying the surgical procedure for device implantation. Second, in order to support a variety of experiments (e.g., drug evaluation) using a rodent animal model, we present a special WPT transceiver system with a relatively large power transmitter and a miniature implantable power receiver. We present a multi-coil design that allows steady power transfer from the floor of an animal cage to the bodies of a group of free-moving laboratory rodents.

Keywords: implantable device, wireless power transfer, animal experiment, power transmitter, power receiver, antenna, double-helix coil, blood vessel, nervous system, resonance, even magnetic field, miniaturization

1. Introduction

Diagnosis and treatment of human diseases using an implantable electronic device represent a new trend in modern medicine. While the developments of biosensors, bioelectric stimulators and drug release mechanisms are important in the designs of medical implants, these developments are application specific. Therefore, they cannot be studied in a unified fashion. On the other hand, essentially all implantable devices require a common component: a power supply, which is usually a battery. Recent advances in wireless power transfer (WPT) provide an alternative method to power implantable electronic devices [1–3]. The WPT technology not only eliminates the needs of repeated surgical replacements of a depleted battery

within the human body, but also reduces the size of the implant, simplifies the implantation procedure, and enables the device to be placed in restricted anatomic locations prohibitive to large implants.

Due to the importance of WPT in the next-generation medical implants, there have been extensive studies over recent years [4–7]. One of the major limiting factors in battery-less implants is the low power output at the receiving end due to the weak coupling of the wireless power link. Many existing WPT components in biomedical implants operate in the low-MHz frequency range, e.g., those utilizing the widely accepted 13.56 MHz industrial, scientific, and medical (ISM) band. Although the WPT component in this frequency range is easy to design and robust, a relatively large receiver antenna is required, which limits its application to implantable devices in millimeter scales [8]. In recent years, it has been demonstrated that this challenge can be overcome by increasing the operating frequency and producing spatially focused regions within the biological tissue [9]. This approach effectively makes the WPT component smaller; however, the design of the power receiver coils that both operate in a high frequency and adapt to anatomical features of biological organs or tissues has not been well studied. In essentially all magnetic resonance based WPT systems reported, the power receiver within the implant utilizes a spiral coil in either a planar or a solenoidal form, as shown in **Figure 1a** and **b**, respectively [4–6]. In general, the planar spiral coil (PSC) [4, 5, 7] has been used in implants having a relatively larger surface, such as certain cardiac pacemaker [10]. In other cases, medical implants are often designed in a cylindrical or capsular shape such as the Bion® microstimulator [11]. For these cases, the use of a solenoidal coil is more common [12–14]. Despite successful designs exist, these two forms of coils cannot meet the requirements for all medical implants. For example, the human body has many tubular-shaped organs, such as nerves, lymphatic channels and blood vessels. An implant that wraps around such a biological structure to perform sensing and therapeutic functions is often desirable. In these cases, serious problems are encountered, with rare exceptions, because the structure is not allowed to be cut, and it is difficult to cut and rejoin a solenoidal coil

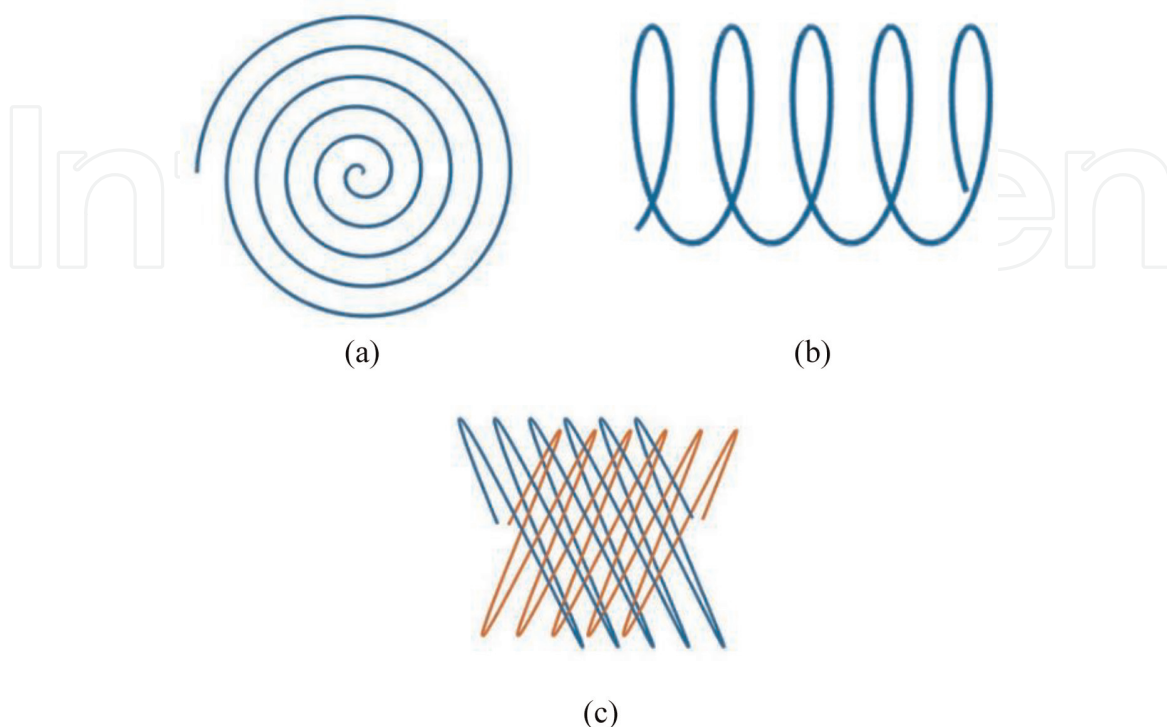


Figure 1.

Power receiver coils within the body: (a) planar spiral coil, (b) solenoidal coil, and (c) DH coil.

during surgery. In addition, the optimal orientation of the implant may not comply with the orientation of the power transmitter coil outside the human body. In order to solve these problems, we will present a new form of coil, called double-helix (DH) coil (**Figure 1c**), to be applied to tubular organs within the human body.

Implantable devices are used not only for diagnosis and treatment of human diseases, but also for developments of new drugs and therapeutic mechanisms (e.g., electric stimulation). In the early stage of these developments, an animal model (e.g., the rodent model) is often utilized to study both treatment efficacies and side effects. In these studies, specially designed microsensors are often implanted within the body of a laboratory rodent to measure certain variables of interest [9]. Frequently, animal behaviors are also monitored by videotaping and other means [15]. This approach often encounters a significant problem of lacking a suitable power supply because the use of either a battery or a wire connection to the implant inside the body seriously interferes with animal's mobility and behavior. In this case, the application of the WPT technology is essential because it allows much reduced weight and size of the system being carried by, or implanted within, the rodent [16]. In order to provide the animal with a sufficient space for free movements, a special WPT system with a large stationary transmitter (in which the coil is embedded under the floor of an animal cage) and a miniature receiver (implanted within or carried by the animal) is required. In order for the WPT system to perform properly regardless of the animal's location within the cage, the transmitter must produce an even radio-frequency (RF) magnetic field throughout the floor of the animal cage. As a result, the wirelessly delivered energy is relatively even everywhere over the entire floor. This chapter studies this problem and presents a seven-coil design with several desirable properties, including the theoretical optimality and ease of implementation.

This chapter is organized as follows. In Section 2, we describe the DH coil that can be applied to tubular organs within the human body. The coupling factor and power transfer efficiency (PTE) were analyzed. To further evaluate the performance of the DH coil, both simulations and experiments were conducted and presented. In Section 3, we present a power mat consisting of an array of planar transmitter coils. This mat produces a nearly even magnetic field distribution over the entire animal cage floor. For clarity, we present our evaluation, simulation and/or experimental results at the end of each methodological section. Finally, we conclude this chapter in Section 4.

2. Double-helix coil for wrap-around implants

The human body contains networks of tubular organs, such as nerves, lymphatic channels and blood vessels [17]. In order to monitor the functions or pathologic states of these organs (e.g., clogging of a certain major blood vessel) or provide therapeutic functions (e.g., stimulating a peripheral nerve), a wirelessly powered miniature implant wrapped around a tubular or rod-like biological structure is highly desirable. Although an ordinary solenoidal coil can support this wrap-around implant, an intact tubular organ usually cannot be cut and rejoined to allow a solenoidal coil to be threaded into the desired implanting position. Alternatively, one may wind the coil wire around the tubular organs manually during surgery. This method is practically unacceptable due to the restricted time of surgery and difficulties in quality control manual winding. Another method is to wrap the tubular organ by a coil that has been cut longitudinally. To reform an intact coil, a surgeon needs to reconnect the wires by soldering or using special connectors. This approach is also unrealistic due to the high risk of infection involved and the possible failure of the connectors.

In addition to these practical difficulties, the usage of a solenoidal coil for wrap-around implants suffers from another implementational problem. In most cases, it is desirable to use a flexible PSC for the power transmitter because this planar coil can be easily integrated with a garment, a blanket or a bedding sheet, providing a high convenience for unobtrusive recharging of the implant. In order to achieve the maximum coupling between the transmission and reception coils, the solenoidal coil of the implant is expected to be oriented perpendicularly to the body surface (**Figure 2a**). This requirement is highly problematic because, as indicated by human anatomy [17], many tubular organs within the body are oriented parallel to the body surface, which provides the worst orientation to the PSC for power transmission because of the weakest magnetic coupling (**Figure 2b**).

To address these significant problems, we have developed an air-core DH coil for tubular implants [18, 19]. The new coil can be printed on a flat flexible printed circuit board (PCB) and installed on a tubular biostructure during surgery. As shown in **Figure 3**, when the DH coil is wrapped around a tubular organ parallel to the skin surface, the optimal coupling can be achieved with a PSC integrated with a garment or a bedding sheet.

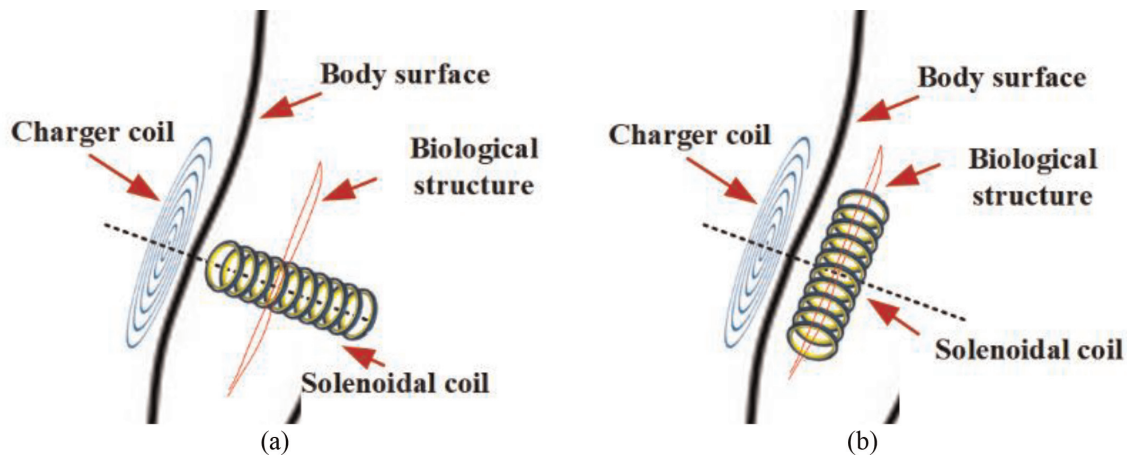


Figure 2. The implanted solenoid coil (a) perpendicular and (b) parallel to a planar transmitter (shown in blue).

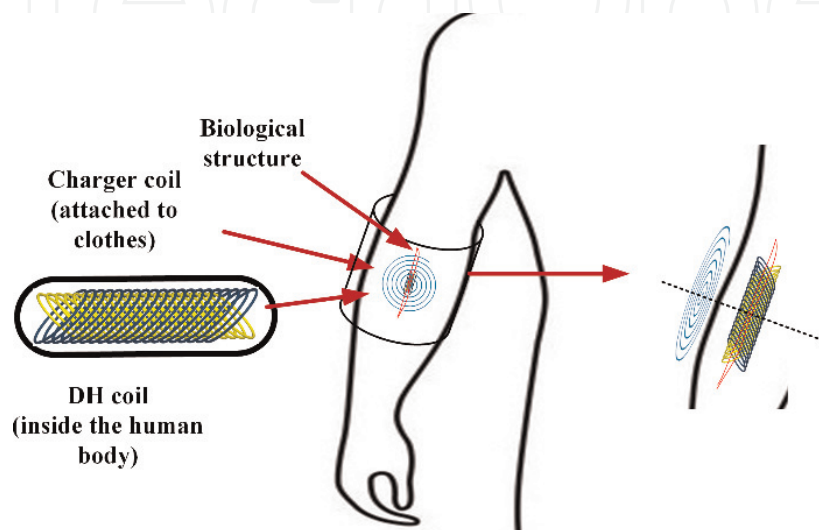


Figure 3. A DH coil is wrapped around a biological structure (red curve) to serve as a power receiver.

2.1 Structural design of DH coil

Figure 4a shows a set of parallel sinusoidal wires printed on both sides of a flexible PCB. This PCB is made of polyimide film which is characterized by high strength, low RF energy loss, small thickness, and high flexibility. The wires on two sides are connected to each other in series via a column of through holes (one of them is shown), forming closed loops. The current paths are denoted by the black arrows in **Figure 4a**. In addition to the DH coil, sensors, actuators, microprocessor and electronic elements (not shown) can be installed on the same flexible PCB. During surgery, the hermetically sealed PCB (using a biocompatible polymer material) is wrapped around the tubular structure at the position of interest forming a double helix winding along with all electronic components, as shown in **Figure 4b**. It can be observed that, after the tubular structure is formed, the closed loops on the two sides of the PCB form opposite tilt angles but maintain the clockwise/counterclockwise current direction.

The two-layer structure in **Figure 4** can be extended to a multiple-layer structure using a PCB with more than two layers. Similarly, the 45° tilted angle in each layer can be modified to adapt to specific tubular organ orientation for optimal wireless power delivery.

2.2 Inductance and mutual inductance of DH coil

As shown in **Figure 5**, for simplicity, the DH coil is separated into several cells and each cell consists of an inner loop (Loop 1) and an outer loop (Loop 2).

By superposition, the inductance of the DH coil is equal to the sum of the cell inductance and the mutual inductance between each cell (**Figure 5a**), namely:

$$L_{DH} = \sum_{i=1}^n \sum_{\substack{j=1 \\ j \neq i}}^n M_{i,j} + \sum_{i=1}^n L_i = \sum_{i=1}^n \sum_{\substack{j=1 \\ j \neq i}}^n M_{i,j} + nL_{cell}. \quad (1)$$

where $M_{i,j}$ denotes the mutual inductance between cell i and cell j , and L_{cell} denotes the inductance of a single cell.

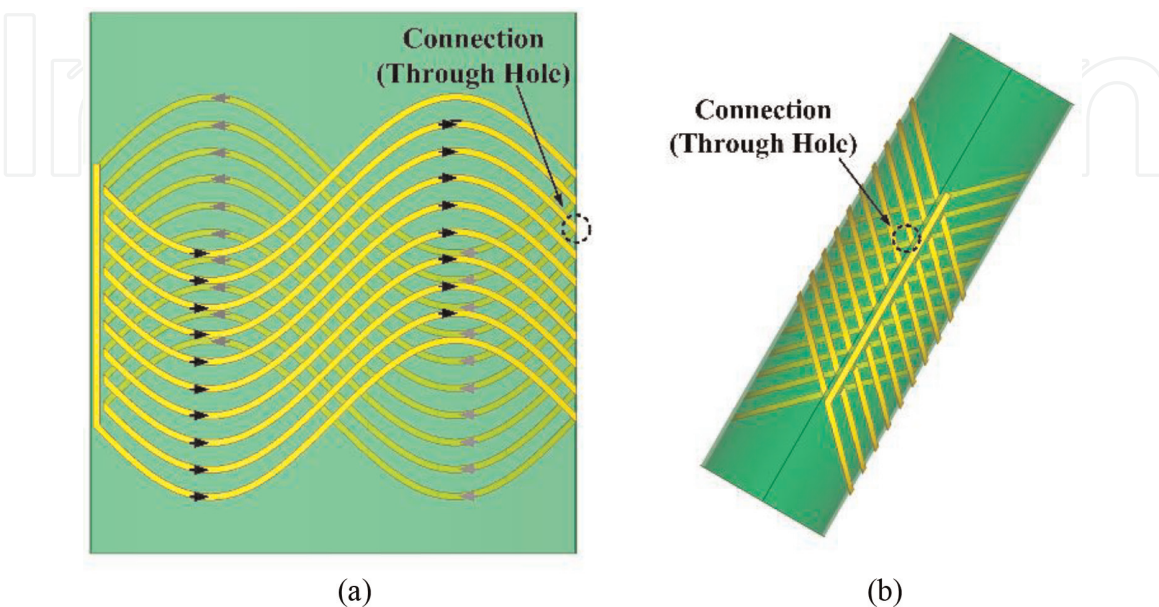
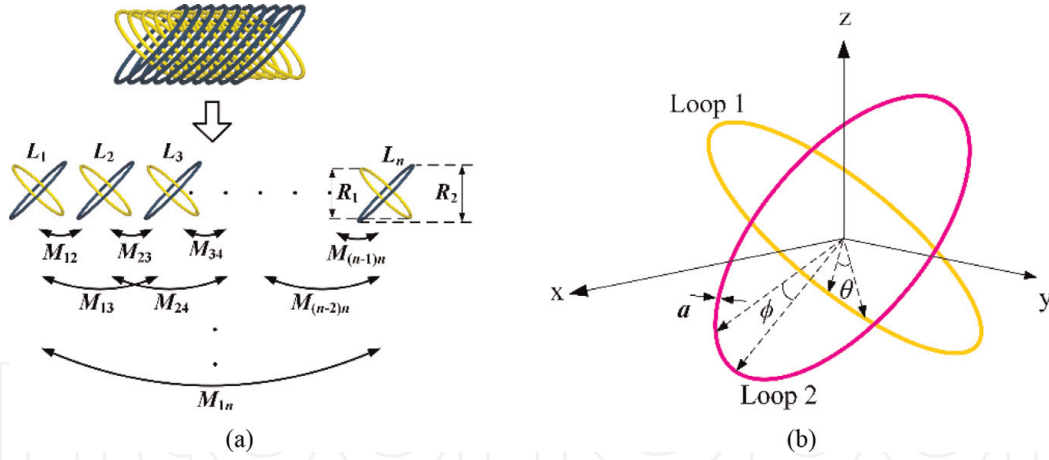


Figure 4.
 (a) Schematic representation of the DH coil and current directions indicated by arrows. Conductors are printed on both sides of the flexible PCB; (b) the PCB is wrapped to form a DH coil.


Figure 5.

(a) The DH coil can be separated into n cells, having mutual inductance with each other; (b) cell model.

According to the cell model (**Figure 5b**), the inductance of a single cell is the sum of the inductances of Loops 1 and 2 and their mutual inductance. Since the loops are perpendicular to each other, the mutual inductance between the loops is zero so that the inductance of a single cell is given by

$$L_{cell} = L_1 + L_2 + 2M_{12} = L_1 + L_2 \quad (2)$$

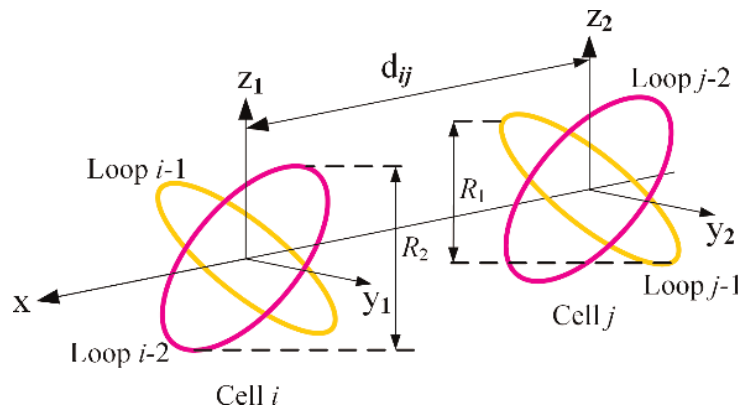
where L_1 and L_2 are the inductances of Loops 1 and 2, respectively, given by

$$\begin{cases} L_1 = \frac{\mu_0}{4\pi} \int_0^{2\pi} \int_0^{2\pi} \frac{R_1(R_1-a)(2 \sin \theta \sin \phi + \cos \theta \cos \phi)}{\sqrt{2(R_1 \cos \theta - (R_1-a) \cos \phi)^2 + (R_1 \sin \theta - (R_1-a) \sin \phi)^2}} d\theta d\phi \\ L_2 = \frac{\mu_0}{4\pi} \int_0^{2\pi} \int_0^{2\pi} \frac{R_2(R_2-a)(2 \sin \theta \sin \theta' + \cos \theta \cos \theta')}{\sqrt{2(R_2 \cos \theta - (R_2-a) \cos \phi)^2 + (R_2 \sin \theta - (R_2-a) \sin \phi)^2}} d\theta d\phi \end{cases} \quad (3)$$

where R_1 and R_2 are the projected radii of Loops 1 and 2 along the z axis (**Figure 5a**).

Figure 6 shows a model containing two cells. The mutual inductance between the two cells is calculated by

$$\begin{aligned} M_{i,j} &= M_{i-1,j-1} + M_{i-1,j-2} + M_{i-2,j-1} + M_{i-2,j-2} \\ &= M_{i-1,j-1} + 2M_{i-1,j-2} + M_{i-2,j-2} \end{aligned} \quad (4)$$


Figure 6.

Modeling of the mutual inductance between two cells.

where,

$$\begin{cases} M_{i-1,j-2} = \frac{\mu_0}{4\pi} \int_0^{2\pi} \int_0^{2\pi} \frac{R_1 R_2 \cos \theta \cos \phi}{\sqrt{(R_1 \cos \theta - R_2 \cos \phi + d_{ij})^2 + R_1^2 + R_2^2 + 2R_1 R_2 \cos(\theta + \phi)}} d\theta d\phi \\ M_{i-1,j-1} = \frac{\mu_0}{4\pi} \int_0^{2\pi} \int_0^{2\pi} \frac{R_1^2 (2 \sin \theta \sin \phi + \cos \theta \cos \phi)}{\sqrt{(R_1 \cos \theta - R_1 \cos \phi + d_{ij})^2 + 2R_1^2 - 2R_1^2 \cos(\theta - \phi)}} d\theta d\phi \\ M_{i-2,j-2} = \frac{\mu_0}{4\pi} \int_0^{2\pi} \int_0^{2\pi} \frac{R_2^2 (2 \sin \theta \sin \phi + \cos \theta \cos \phi)}{\sqrt{(R_2 \cos \theta - R_2 \cos \phi + d_{ij})^2 + 2R_2^2 - 2R_2^2 \cos(\theta - \phi)}} d\theta d\phi \end{cases} \quad (5)$$

Therefore, the total inductance of the DH is derived based on the superpositions of the calculated inductances by Eq. (2).

As shown in **Figure 7a**, the mutual inductance between the DH coil and the transmitter (Tx) can also be regarded as the sum of all individual mutual inductances between Tx and each loop in the DH coil, namely,

$$M_{Total} = \sum_{i=1}^n M_{Ti-1} + \sum_{i=1}^n M_{Ti-2} = \sum_{i=1}^n (M_{Ti-1} + M_{Ti-2}) = \sum_{i=1}^n M_{Ti} \quad (6)$$

where M_{Ti-1} and M_{Ti-2} are the mutual inductances between Tx and the i th inner and outer loops, respectively, M_{Ti} is the mutual inductance between Tx and the i th cell, and n denotes the cell number. For simplicity, Tx is modeled as a circular coil with only one turn as shown in **Figure 7b**.

Then, M_{Ti-1} and M_{Ti-2} are given by

$$\begin{cases} M_{Ti-1} = \frac{\mu_0 m}{4\pi} \int_0^{2\pi} \int_0^{2\pi} \frac{R_1 R_{TX} \cos(\theta - \gamma)}{\sqrt{(R_1 \cos \theta - R_{TX} \cos \gamma)^2 + (-R_1 \sin \theta - R_{TX} \sin \gamma)^2 + (R_1 \cos \theta - d)^2}} d\theta d\gamma \\ M_{Ti-2} = \frac{\mu_0 m}{4\pi} \int_0^{2\pi} \int_0^{2\pi} \frac{R_2 R_{TX} \cos(\phi - \gamma)}{\sqrt{(R_2 \cos \phi - R_{TX} \cos \gamma)^2 + (-R_2 \sin \phi - R_{TX} \sin \gamma)^2 + (R_2 \cos \phi + d)^2}} d\phi d\gamma \end{cases} \quad (7)$$

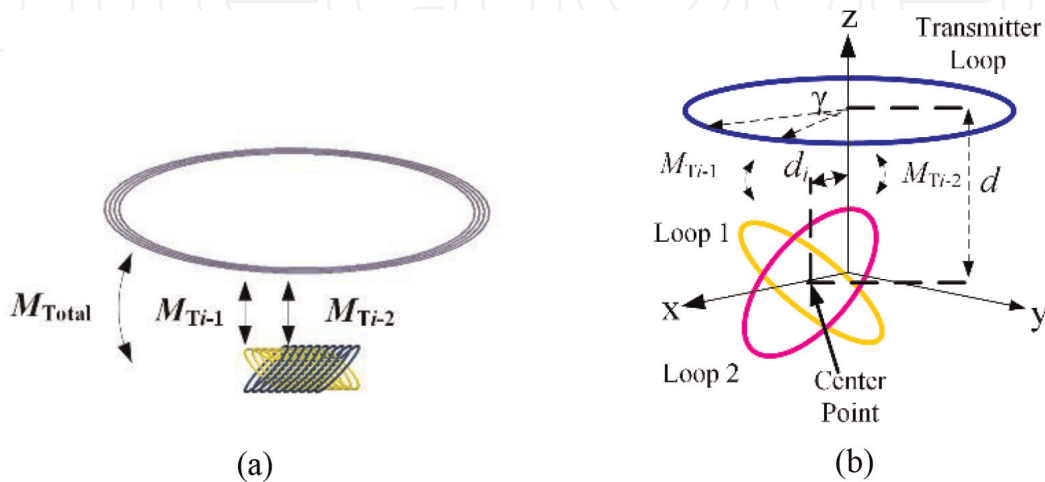


Figure 7.
 (a) The total mutual inductance between Tx and the DH coil is calculated by the superpositions of the mutual inductances between Tx and all cells; (b) Modeling of the mutual inductance between Tx and one cell.

where R_{TX} is the radius of Tx, μ_0 is the magnetic permeability of free space, and d is the vertical distance between the cell and Tx. Accordingly, we have

$$M_{Ti} = M_{Ti-1} + M_{Ti-2}. \quad (8)$$

The coupling factor k between Tx and Rx is given by

$$k = \frac{M_{Total}}{\sqrt{L_{DH}L_{TX}}} \quad (9)$$

where

$$L_{TX} = \mu_0 R_{TX} \left(\ln \left(\frac{R_{TX}}{a_{TX}} \right) - 1.75 \right). \quad (10)$$

2.3 Coupling factor simulations

According to the magnetic resonant WPT theory, the coupling factor k largely influences system performance [20]. In order to evaluate the coupling factor in the system with the misalignment between the transmitter and receiver coils, the proposed DH coil was compared to a conventional double-layer solenoid by simulation. The transmitter was modeled as a PSC with the outer and inner radii being 30 and 15 mm, respectively. For the DH coil and conventional solenoid, R_1 and R_2 were 5 and 6 mm, respectively. The variation of k was investigated with respect to the lateral and angular misalignments.

Figure 8 shows the simulation models with lateral or angular misalignments. X_0 and Y_0 in **Figure 8a** and **b** indicate the displacements along the x-direction and y-direction, respectively. α and β indicate the rotating angles around the x-axis and y-axis, respectively. The vertical distance d in **Figure 8c** and **d** is 20 mm in all cases. The simulation was used to calculate the coupling factor in different scenarios. The results are shown in **Figure 9**.

It is seen that offers the maximum coupling factor k of the conventional solenoid much smaller than that of the DH coil, comparing **Figure 9a** and **b**. Additionally, the coupling factor k of the DH coil is larger than that of the conventional solenoid in most of the measurement range. **Figure 9c** showed that k is essentially invariable as the conventional solenoid rotates around the x-axis. However, the DH coil has an optimal angle as which the largest k is achieved. With β decreases, the central axes of both the DH coil and conventional solenoid change from being perpendicular to being parallel with the plane of Tx as shown in **Figure 9d**. Within such a process, the coupling factor of the solenoid decreases, while the coupling factor increases for the DH coil. In addition, when β is 0, the coupling factor of the DH coil is much larger than that of the conventional solenoid. Accordingly, the orthogonal-coil structure enhances the mutual inductance. This phenomenon verifies the superiority of the DH coil over the traditional solenoid.

2.4 Experimental results

We constructed several prototypes of DH coils with variable turns, gaps and widths. Then, the coil with the largest quality factor was chosen and tuned to a resonant frequency of 5.2 MHz using capacitors. This DH coil is presented in **Figure 10**.

To study WPT performances in different misalignment scenarios, the PTE was chosen as an evaluation index. The PTE was measured based on the scatter

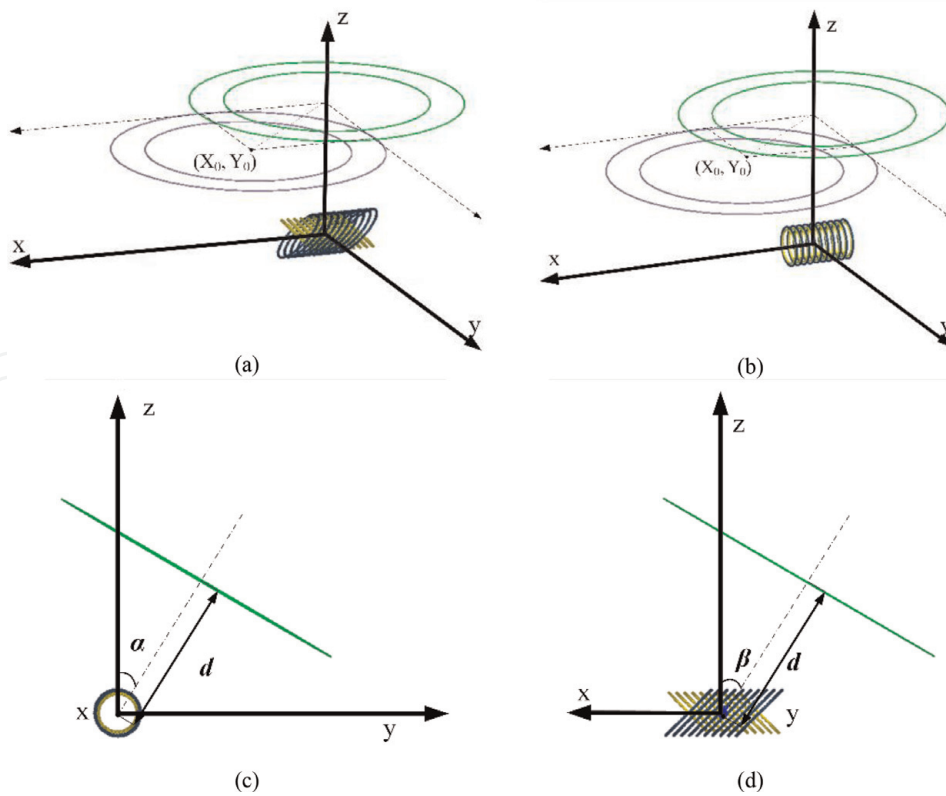


Figure 8. Simulation models of (a) DH coil and (b) solenoid coil for lateral misalignment, and for angular shifting around (c) the x-axis and (d) the y-axis, respectively.

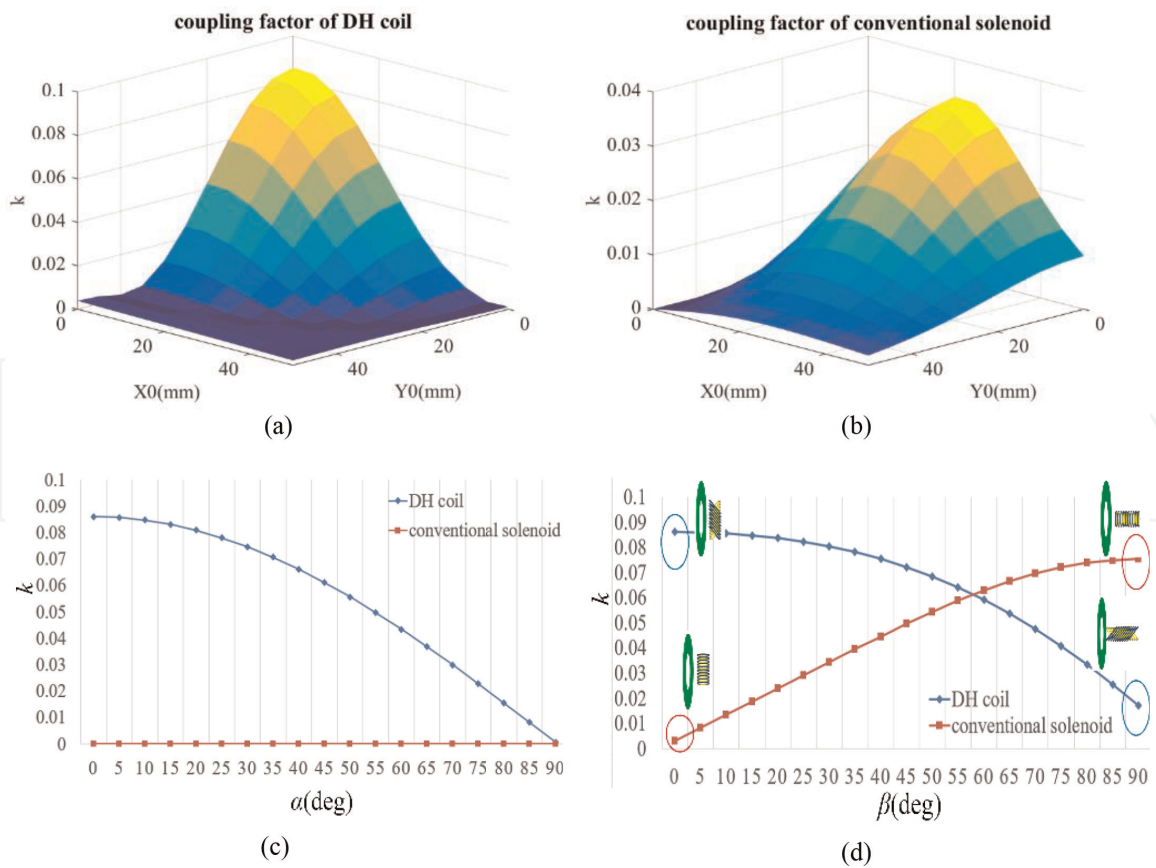


Figure 9. The coupling factor as a function of the relative position between the receiver and transmitter coils in different cases: (a) DH coil with lateral misalignment, (b) traditional coil with lateral misalignment, (c) the angular shifting around the x-axis, and (d) the angular shifting around the y-axis.

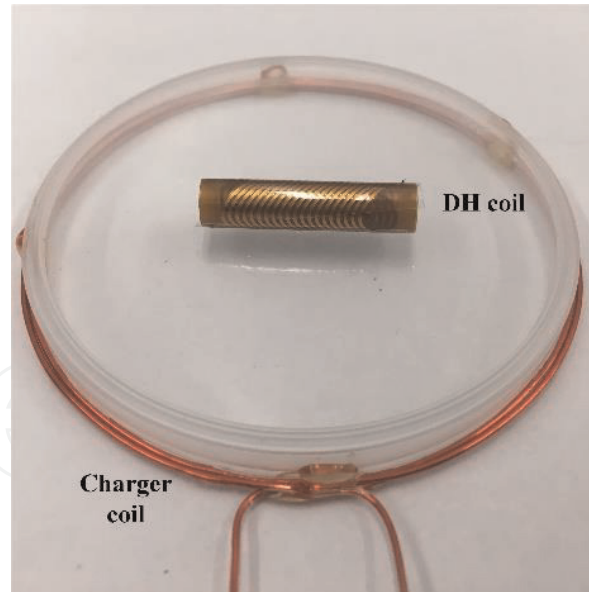


Figure 10.
Experimental setups for efficiency measurement.

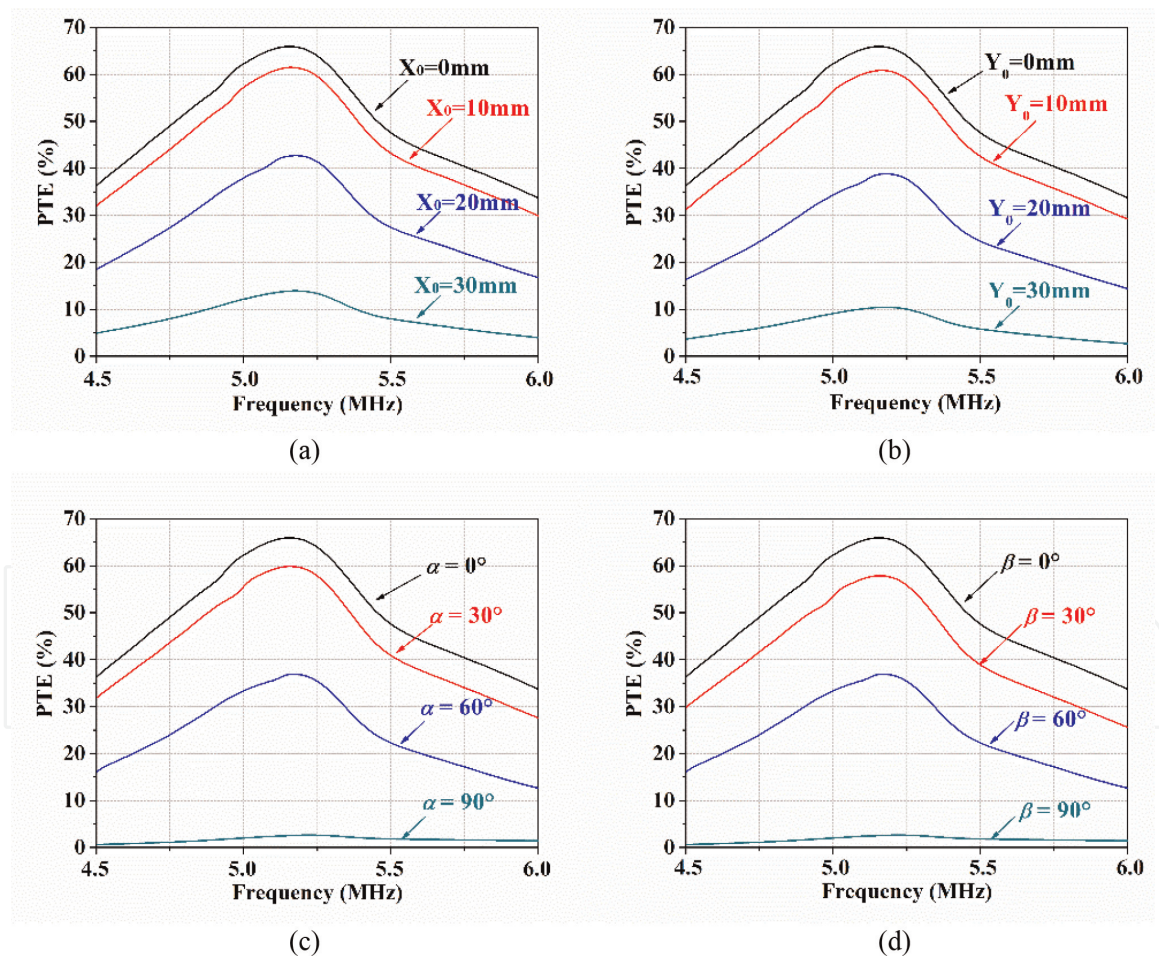


Figure 11.
PTE measurements vs. frequency with variable misalignments: (a) lateral misalignment in the x-direction, (b) lateral misalignment in the y-direction, (c) angular misalignment around x-axis, and (d) angular misalignment around y-axis.

parameters measured by a network analyzer. PTE measurements were also performed for both lateral and angular misalignments. The results shown in **Figure 11** indicate that the WPT system achieves the maximum PTE at the resonant

frequency. However, the PTE decreases as the misalignment increases, similar to the variation of the coupling factor.

It can be observed that the PTE is strongly dependent on the inductive coupling, which was discussed in the previous section. Therefore, the proposed DH coil offers more efficient power delivery than the traditional solenoid.

3. Mat-based wireless power transfer to moving targets

Neural stimulation and recording provide emerging prosthetic and treatment options for spinal cord injury, stroke, sensory dysfunction, and other neurological diseases and disorders. Neural recording from awake animals with observable behavior has greatly enhanced our understanding of central and peripheral nervous systems. Although there has been substantial studies on miniaturized, implantable electronic circuits that record neural data and stimulate neuronal networks in freely moving laboratory animals, the mobility of the animal subject is often limited, and the experimental results obtained under restricted conditions may not reflect the full repertoire of brain activity corresponding to their natural behaviors [16]. There are similar problems in the study of new drugs which often requires monitoring a number of variables from the inside of the animal body and observation of their mobility and behaviors.

Traditionally, magnetic induction was used for WPT using a similar form to a transformer [21]. This form of the magnetic induction method is highly efficient (>90%) in the near-field range, but much less efficient as the transmission distance increases. In 2007, an efficient mid-range WPT via strongly coupled magnetic resonance was reported [22]. This system consists of four coils (**Figure 12**), namely, driver, primary (or transmitter), secondary (or receiver), and load coils. Inductive coupling is used between the driver and primary coils as well as between the secondary and load coils. The primary and secondary coils with the same resonant frequencies tend to exchange energy efficiently. This mechanism is valuable in the application to medical implants because biological tissues are generally non-resonant at the operating frequency in the RF range.

Because our special WPT system involves moving targets (animals, e.g., rodents), the vertical component of the magnetic field generated by the transmitter is required to be distributed as even as possible over the entire area of interest (e.g., floor of the rodent cage). When this condition is satisfied, the device carried by or implanted within each rodent can receive steady power at any location of the floor. Previously, we designed a WPT system in which multiple circular spiral coils were printed on hexagonal PCBs [23]. These PCBs were then tiled hexagonally forming a “power mat” shown in **Figure 13**. Note that the use of hexagons in the pack of coils is not an arbitrary choice, rather it has been proven that this design will leave the

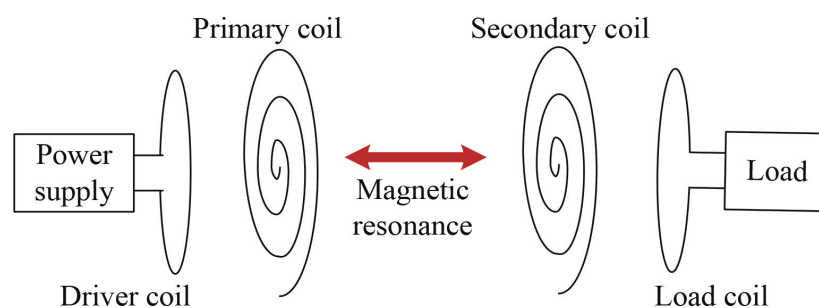


Figure 12. A resonance based WPT system including four coils, namely driver, primary, secondary, and load coils.

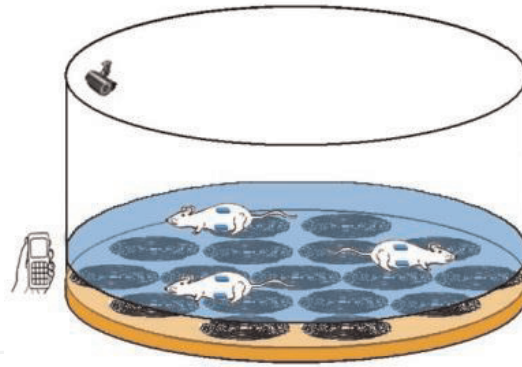


Figure 13.
WPT system in which the floor of the animal cage is located over a hexagonally packed power mat.

smallest gap between circular resonator coils [24]. The power mat is able to deliver wireless power to the implants and “carry-on” devices to multiple rodents which move freely on the floor above the mat.

It has been found from computer simulation that the packing of a circle by identical disks demonstrates interesting patterns [25]. Denser packings consist of specific numbers of disks. The first several numbers are: 1, 7, 19, 37, 61, and 91. Although the packing density increases as more disks are packed within the enclosing circle, the density is upper-bounded by $\pi^2/12 \approx 0.822$. Although, in general, using more disks produces a higher density, the implementation complexity increases as the number of disks increases. Additionally, it is difficult to connect the RF signal to numerous transmitter (Tx) coils, and the cost involved is high. On the other hand, we have previously reported that the RF signal can be easily connected to a pair of open concentric rings to power seven Tx coils simultaneously [23]. Therefore, if more than one coil is used in the Tx, the seven-coil design is often the best choice for most practical applications to power free-position devices although its packing density is not the highest.

3.1 Theoretical analysis of mat-based WPT system

As shown in **Figure 14**, the mat-based WPT system enables magnetically coupled resonance between an array of transmitter coils and a single receiver coil.

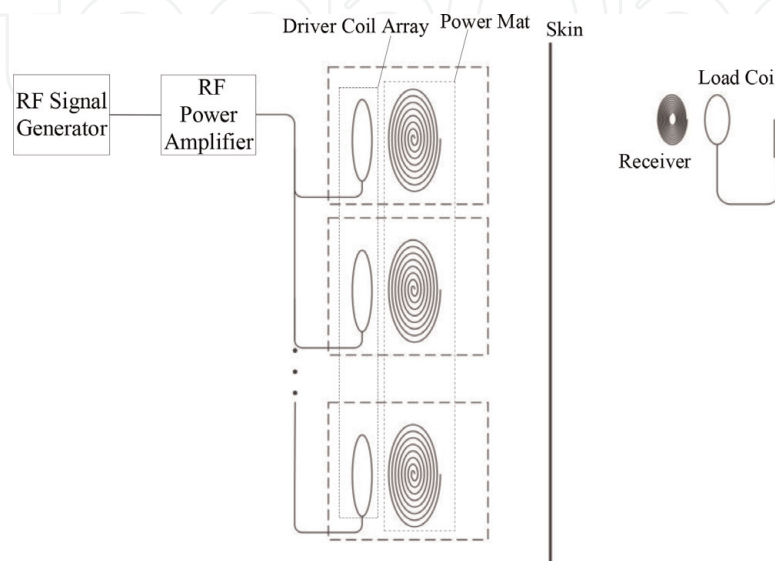


Figure 14.
Mat-based WPT system design.

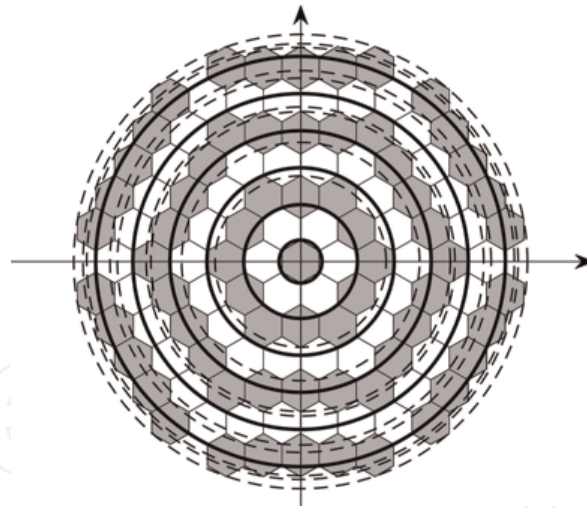


Figure 15.
 A large hexagonally packed power mat.

An adjustable RF oscillator produces a sinusoidal signal, which is amplified by a power amplifier. The output of the amplifier is connected to an array of driver coils which are inductively coupled with primary coils [23]. At the power receiving site (a laboratory animal), the receiver coil is inductively coupled with a load coil to supply the power to the electronic components within the implant.

In the coupled mode theory (CMT), the first eigen-mode is used to analyze a resonant system. The approximation by the first eigen-mode is quite accurate under the condition of a strong coupling in the WPT system. In practical applications, it is not possible or necessary to directly work on an arbitrary large number of resonators. Rather, for a large hexagonally packed transmitter (HPT) mat (**Figure 15**), every one of the resonators can be treated as in the middle of the mat, except for those ones at the edge, and fortunately the edge effect can be solved simply by making the mat larger than the animal cage floor. For this reason, we may simplify analysis by examining the seven-resonator case.

Let us index the seven transmitters from 1 to 7 and the single receiver have an index of 8. In order to describe the strongly coupled system, a set of differential equations based on CMT is given by [22].

$$\begin{aligned} \dot{a}_8(t) &= (j\omega_0 - \Gamma_8 - \Gamma_L)a_8(t) + \sum_{j=1}^7 j\kappa_{ij}a_j(t) \\ \dot{a}_i(t) &= (j\omega_0 - \Gamma_i)a_i(t) + \sum_{\substack{j=1 \\ j \neq i}}^8 j\kappa_{ij}a_j(t) + f_i(t), \quad i = 1, \dots, 7 \end{aligned} \quad (11)$$

Or, if written in matrix form

$$\begin{bmatrix} \dot{a}_1(t) \\ \dot{a}_2(t) \\ \vdots \\ \dot{a}_7(t) \\ \dot{a}_8(t) \end{bmatrix} = \begin{bmatrix} (j\omega_0 - \Gamma_1) & j\kappa_{12} & \cdots & j\kappa_{17} & j\kappa_{18} \\ j\kappa_{21} & (j\omega_0 - \Gamma_2) & \cdots & j\kappa_{27} & j\kappa_{28} \\ \vdots & \vdots & \ddots & \vdots & \vdots \\ j\kappa_{71} & j\kappa_{72} & \cdots & (j\omega_0 - \Gamma_7) & j\kappa_{78} \\ j\kappa_{81} & j\kappa_{82} & \cdots & j\kappa_{87} & (j\omega_0 - \Gamma_8 - \Gamma_L) \end{bmatrix} \begin{bmatrix} a_1(t) \\ a_2(t) \\ \vdots \\ a_7(t) \\ a_8(t) \end{bmatrix} + \begin{bmatrix} f(t) \\ f(t) \\ \vdots \\ f(t) \\ 0 \end{bmatrix} \quad (12)$$

where $a_i(t)$, $i = 1, 2, \dots, 7$, and $a_8(t)$ are, respectively, the first eigenmodes of the transmitter and receiver resonators corresponding to the natural frequency ω_0 , Γ_i s are the intrinsic loss rates of resonators due to absorption and radiation, Γ_L represents the rate of energy going into the load, κ s are pairwise coupling coefficients between resonators, and f_i s are the inputs to the transmitter resonators. In our case, all f_i s are the same, i.e., $f_1 = f_2 = \dots = f_7 = f$. Note that a_i s are also known as positive frequency components in terms of CMT. Although a_i (generally complex-valued) does not represent a voltage or current directly, the energy contained in each resonator can be represented as $|a_i|^2$, and the power output of the system is $2\Gamma_L|a_8|^2$. Using the CMT concept, the goal of obtaining a uniform power output becomes finding a constant $|a_8|$ within the WPT space.

To make Eq. (12) more concise, we write it into the following form:

$$\dot{\mathbf{a}} = \mathbf{A}\mathbf{a} + \mathbf{f} \quad (13)$$

where the vectors and matrices are in correspondence with Eq. (12).

If the WPT system is driven by a sinusoidal input, e.g., $\mathbf{f}(t) = Fe^{j\omega_0 t}[1, 1, \dots, 1, 0]^T$, the positive frequency components have the form of $\mathbf{a}(t) = \mathbf{a}e^{j\omega_0 t}$ at the steady state. Substituting this into Eq. (13), we can solve for $\mathbf{a}(t)$

$$\mathbf{a}(t) = -\mathbf{B}^{-1}\mathbf{f}(t) \quad (14)$$

where

$$\mathbf{B} = \begin{bmatrix} -\Gamma_1 & j\kappa_{12} & \cdots & j\kappa_{17} & j\kappa_{18} \\ j\kappa_{21} & -\Gamma_2 & \cdots & j\kappa_{27} & j\kappa_{28} \\ \vdots & \vdots & \ddots & \vdots & \vdots \\ j\kappa_{71} & j\kappa_{72} & \cdots & -\Gamma_7 & j\kappa_{78} \\ j\kappa_{81} & j\kappa_{82} & \cdots & j\kappa_{87} & -\Gamma_8 - \Gamma_L \end{bmatrix}$$

In case where \mathbf{B} is not invertible, its pseudo inverse can be used instead. Thus, given Γ_i , κ_{ij} , and f_i , we can compute $a_i(t)$ analytically by Eq. (14). The CMT approach provides a powerful analytical tool for the multi-resonator WPT system. For example, it has been utilized to maximize the efficiency of power transfer and investigate the relay effect by inserting one or more resonators between the transmitter and receiver [26]. Using CMT, we have studied the dynamics of the system involving an array of resonators [27]. Although the previous studies have shown that CMT well characterizes the temporal behavior of the WPT system, it has clear limitations when the system parameter changes. For example, when the receiving resonator moves over the HPT mat, the coupling coefficients κ_{8i} ($i = 1, 2, \dots, 7$) change, and the variations of the system behavior are difficult to determine analytically. In order to study the motion effect of the receiving resonator and answer the critical question whether the receiver resonator can harvest sufficient amount of power at different locations over the HPT mat, we performed numerical simulation and conducted an experimental test.

3.2 Simulation of mat-based WPT system

For a clear illustration of the design principle of the mat-based WPT system, we simulated a single HPT cell consisting of seven PSCs, as limited by the computational complexity. This simulation does not cause a loss of generality because the

results of multiple cells can be obtained simply by superposition of single cell results. In most cases, changes in the position of a device lead to a variation in mutual inductance which results from a change in the magnetic field distribution. Although some unevenness in the distribution is unavoidable, we expect this distribution to be nearly uniform with enhanced misalignment tolerability for WPT applications involving moving targets.

We utilize the concentric model to approximate the coil where the total magnetic field is a superposition of the fields of individual loops in the coil. Assuming that a loop with a radius of a is centered at the origin carrying a current I . Based on the Biot-Savart law, the x-, y- and z-components of the magnetic field at point \mathbf{r} (x, y, z) are given by [28].

$$\begin{aligned} B_x &= \frac{Cxz}{2\alpha^2\beta\rho^2} [(a^2 + r^2)E(k^2) - \alpha^2K(k^2)] \\ B_y &= \frac{Cyz}{2\alpha^2\beta\rho^2} [(a^2 + r^2)E(k^2) - \alpha^2K(k^2)] = \frac{y}{x}B_x \\ B_z &= \frac{C}{2\alpha^2\beta} [(a^2 - r^2)E(k^2) - \alpha^2K(k^2)] \end{aligned} \quad (15)$$

where $\rho^2 = x^2 + y^2$, $r^2 = x^2 + y^2 + z^2$, $\alpha^2 = a^2 + r^2 - 2a\rho$, $\beta^2 = a^2 + r^2 + 2a\rho$, $k^2 = 1 - \alpha^2/\beta^2$, $C = u_0I/\pi$, and $K(\cdot)$ and $E(\cdot)$ are the complete elliptic integrals of the first and second kinds, respectively. For easier calculation, without loss of generality, the current is chosen so that $C = 1$. With the magnetic field of a single loop, we can apply the superposition rule to get the magnetic field generated by a multi-loop circular coil. Since the receiver coil is always in parallel with the transmitter coil (which is installed below the animal cage floor), the fluxes in the receiver coil are contributed by the z-component of the magnetic field. Therefore, we will focus on the z-component of the magnetic field in our analysis.

With these simplifications, we can calculate the magnetic field of the seven-transmitter powering platform. **Figure 16** shows a magnetic field with different distances between the transmitter and the surface (evaluating plane) where the field was evaluated. It can be seen that the separation between the evaluating plane and the transmitter enables the variation of the z-component of magnetic field. When the distance is increasing, the flatness of the magnetic field also improves at first. However, when the height is too large, the magnetic field distribution becomes similar to that of a larger spiral coil, which affects both the flatness and magnitude of the magnetic field. On the other hand, when the height is too small, although the peak magnitude is larger, the z-component is inversed at the gap between resonators, which implies a large fluctuation of the magnetic field.

In order to investigate the effect of mutual inductance between turns in the spiral coil, we also performed a simulation study on the 7-coil mat using a commercial finite element (FE) software HFSS (Ansys Corp., Pittsburgh, PA). **Figure 17** shows the 3D model of the HPT mat used in the simulation, where each PSC was 20 cm in outer diameter, 1 cm in conductive trace width, and 1 cm in trace spacing. The input power was set at 1 W. As stated previously, the goal of the power mat design was to obtain a nearly uniform magnetic field within an extended region to support WPT for moving targets, rather than optimizing PTE (the animal cage is powered from a regular AC socket).

We excited the seven PSCs simultaneously using a common RF power source. Energy was injected into the driver coil array to maintain resonance in the presence of losses and energy drawn from the magnetic field by the receiver coil. **Figure 18** shows the z-component distribution of the magnetic field at 8 and 20 cm distances,

respectively, above the power mat (i.e., the X-Y plane). Color indicates the magnitude of the magnetic field in the z-direction. It can be seen that, at $z = 8$ cm (**Figure 18a**), the magnitude of the magnetic field was the highest (peak) at the center of each coil, and the lowest (valley) at the junction of three coils. When the distance to the HPT mat increased to 20 cm, a smoother magnetic field distribution was observed, but approaching to the field generated by a large spiral coil (**Figure 18b**). In order to evaluate the evenness of distribution quantitatively, the coefficient of variation (COV) was utilized which was defined as the standard deviation of the field values divided by the mean. Thus, a smaller value of the COV indicates a more uniform distribution. **Figure 19** shows the COVs of the magnetic field in the z-direction above the HPT mat at distances from 5 to 40 cm. It can be observed that the COV achieves a value $<10\%$ when the distance is larger than the size of the transmitter coil.

3.3 Receiver coil design

In practical applications, it is almost always beneficial to reduce the size of an implantable device, whereas the WPT system requires a match of the resonant frequencies of the primary and secondary coils. We have designed a new structure of the implantable coil with a miniaturized size while having enough turns to match the resonant frequency of the primary coil. **Figure 20** illustrates our design in which

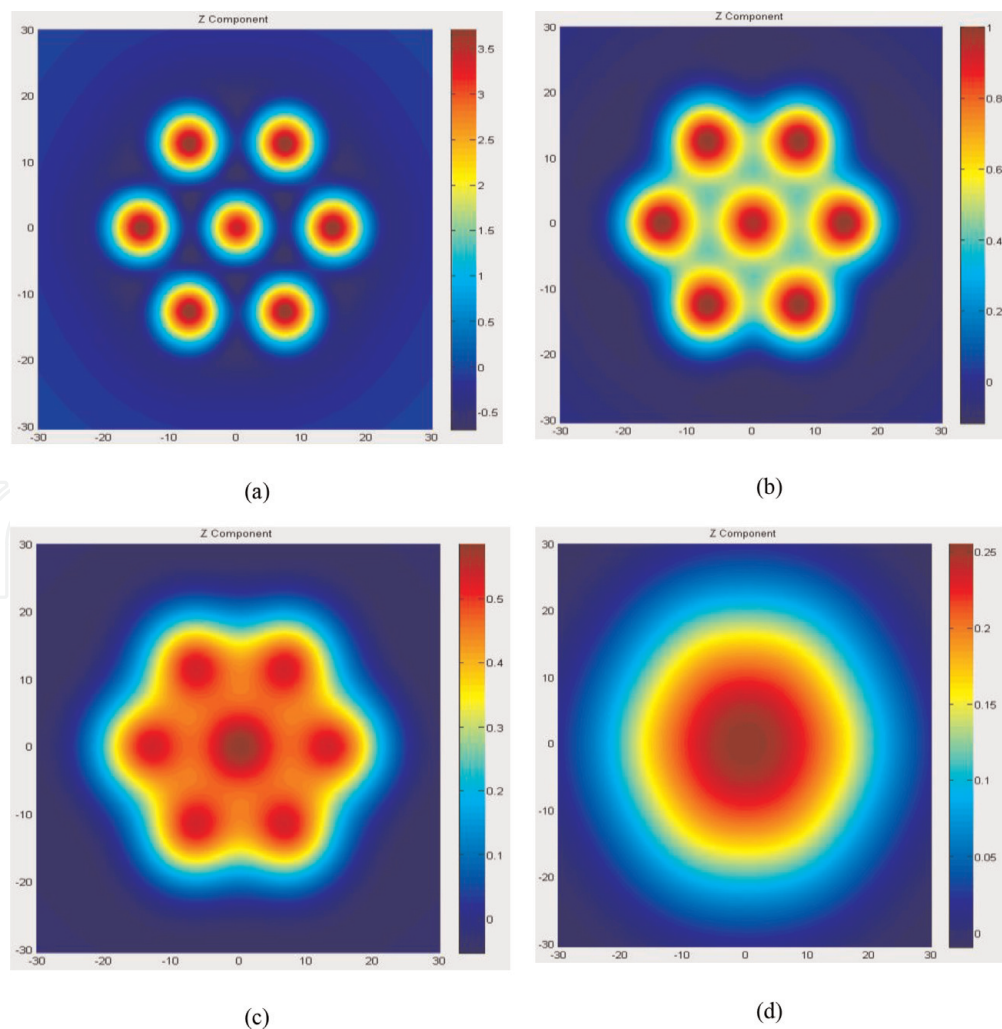


Figure 16. *Z-component of the magnetic field distribution with different separations between the evaluation plane and the transmitter consisting of seven coils. (a) 3.25 cm, (b) 7.25 cm, (c) 10.25 cm, and (d) 20.05 cm.*

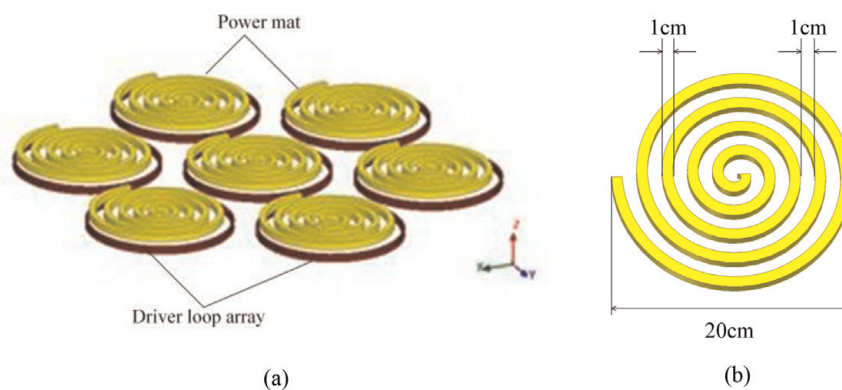


Figure 17. HFSS simulation. (a) 3D model of the transmitter mat; (b) Dimensions of each PSC.

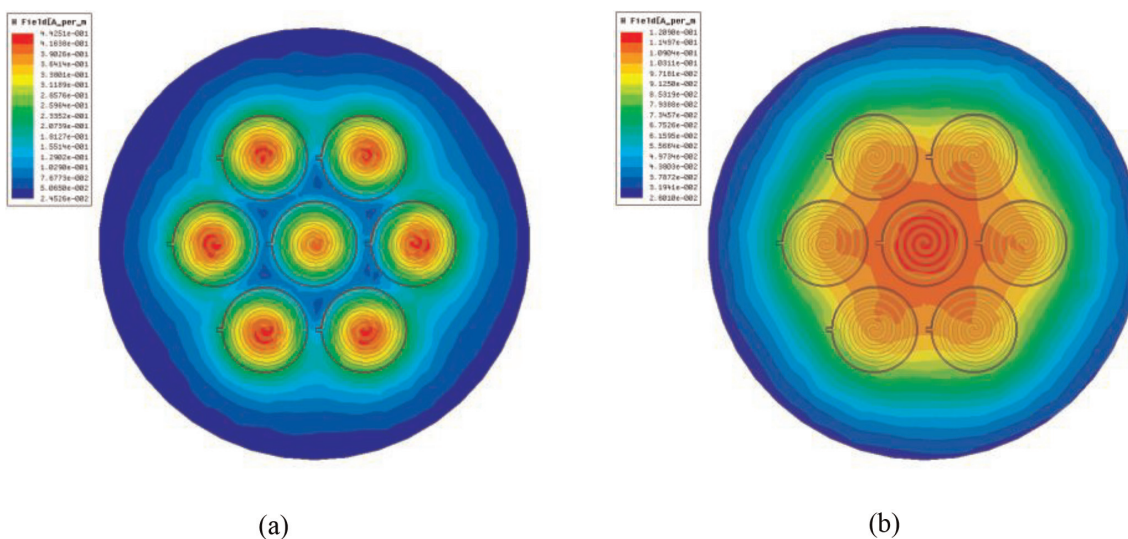


Figure 18. Distribution of the z-component of the magnetic field in a plane at (a) 8 cm and (b) 20 cm above the HPT mat at the resonant frequency of 85.2 MHz.

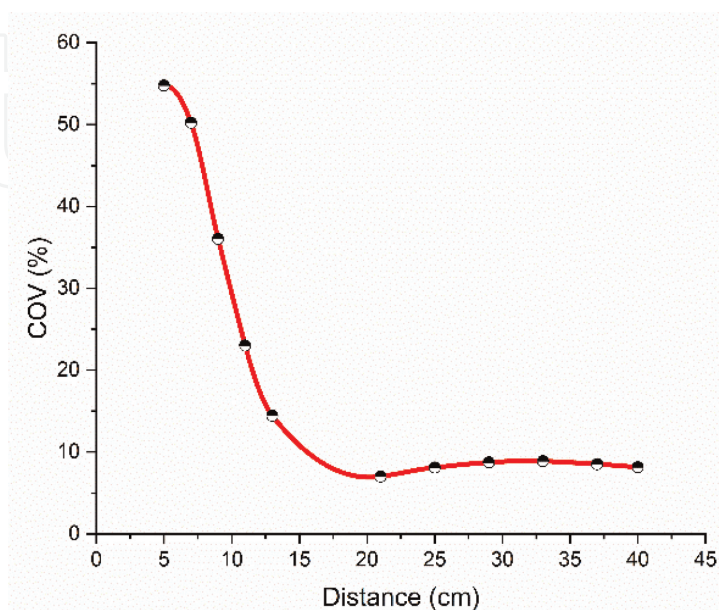


Figure 19. Variation in coefficient of variation (COV) of vertical field distribution as a function of distance above the HPT mat at the resonant frequency of 85.2 MHz.

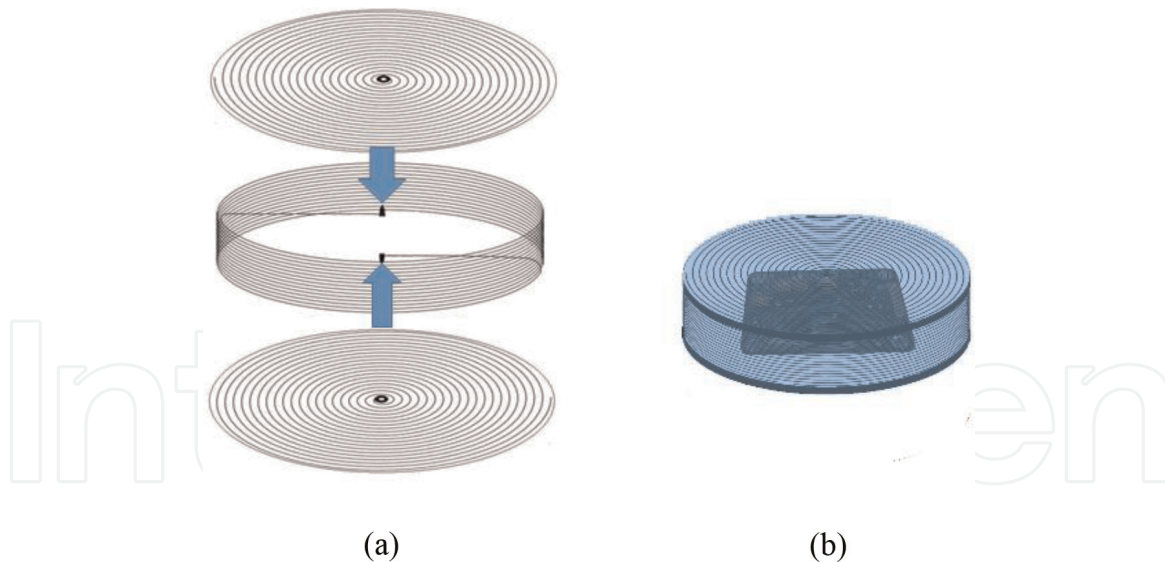


Figure 20.

(a) Three sub-coils wound in proper directions are combined and connected to form a single coil shown in (b).

coils serve as both implant exterior housing and power receiving elements. It consists of two planar sub-coils and one helical sub-coil. The sub-coils are combined into a single coil within a shallow box assembly. By choosing different geometric designs for the sub-coils, different shaped boxes can be obtained. In practical implementation, the exterior of the box must be covered by a biocompatible material for biological safety.

3.4 Experiment tests

In order to study the performance of the mat-based WPT system experimentally, we constructed a prototype mat-based system shown in **Figure 21**, where a transmitter consists of seven circular spiral coils arranged in a hexagonal form. Each PSC was 13.2 cm in diameter, 2.9 mm in trace width, and 1.6 mm in trace spacing. On the reverse side of each PSC, several conductor strips were utilized to form distributed capacitances with respect to the coil on the front side. By changing the numbers of these strips, the resonant frequencies of the PSCs became adjustable. The frequencies were adjusted to 29.453 ± 0.072 MHz with a Q-factor of approximately 100. The prototype of a receiver coil includes three coils and is 25 mm in diameter, 7 mm in height, and 3.39 g in weight. The resonant frequency and Q factor were measured to be 29.075 MHz and 61, respectively.

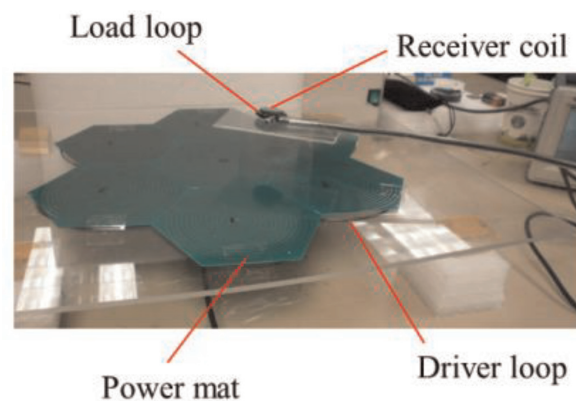


Figure 21.

Experimental platform for measuring magnetic field distribution.

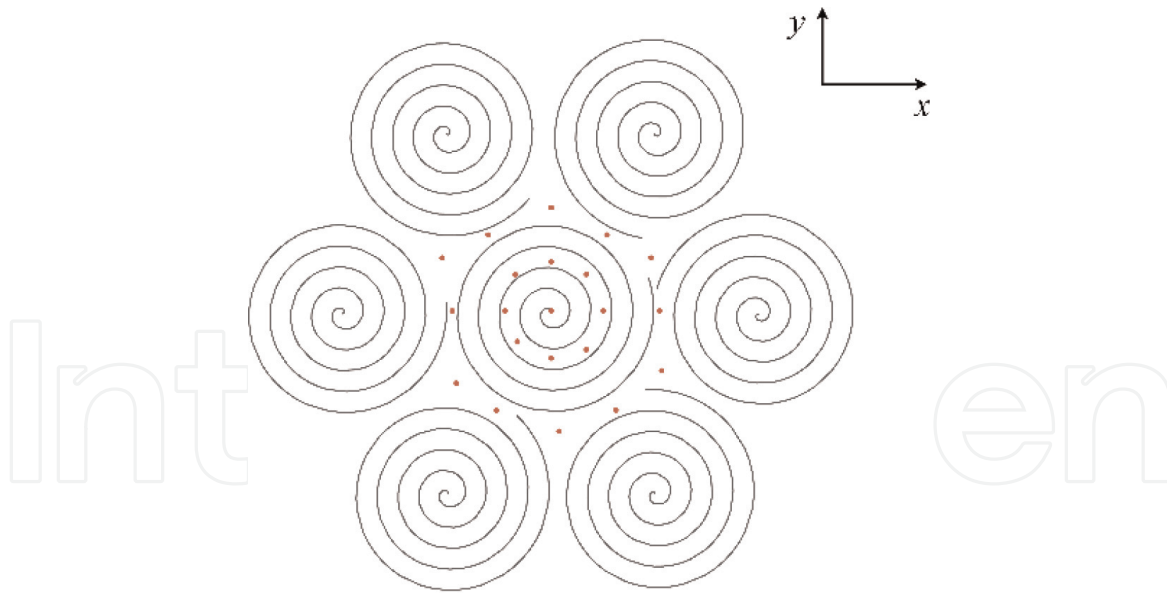


Figure 22.
 Sketch of a seven-resonator mat and the test points.

By measuring the induced voltage in the small receiver coil, the variation of the vertical magnetic field is given by

$$V = -\frac{\partial\varphi}{\partial t} = -N\frac{\partial\bar{B}_z S}{\partial t} \propto B_z \quad (16)$$

When the measuring coil is sufficiently small and the system is driven by sinusoidal input, the induced voltage V in the measuring coil is proportional to the local B_z . As our objective function cancels out the constants relating these two values, we can directly evaluate the cost function using V instead of B_z and compare with the calculation results. As shown in **Figure 22**, these measurement locations were chosen because the magnetic field distribution at any interior PSC in a regular mat can be approximated by the central PSC in each single seven-coil cell (**Figure 15**).

In order to compare the measured voltage with the calculated B_z , we need to normalize both to the same scale, as they are proportional to each other. **Figure 23** shows that the measured data matches the calculated ones very well, except for that the measured data tends to be larger than the calculated ones, which is because the receiver can capture a small portion of horizontal field in addition to the field in the vertical direction. When the measured data are normalized to the center value where the horizontal component is almost zero, the other positions will have larger field than the expected one.

In our WPT system design (**Figure 13**), the separation between the primary and secondary coils includes a distance between the mat and the floor. This distance can be adjusted to achieve both a high WPT performance and an acceptably uniform magnetic field distribution. At different separations, we measured the peak-to-peak values of induced RF voltages in the load coil when the system was powered by a sinusoidal wave at the resonant frequency (approximately 26.6 MHz). Our experiments show that, for our particular system design, the separations of approximately 10 cm and 8 cm between the primary and secondary coils provide a good compromise between performance and magnetic field distribution. In order to visualize this distribution, we interpolated the 21 measured values and plotted the results in **Figure 24**. At a separation of 10 cm, the measured 21 voltage values were in the range between 1.12 and 1.64 V, whereas the mean and standard deviation were

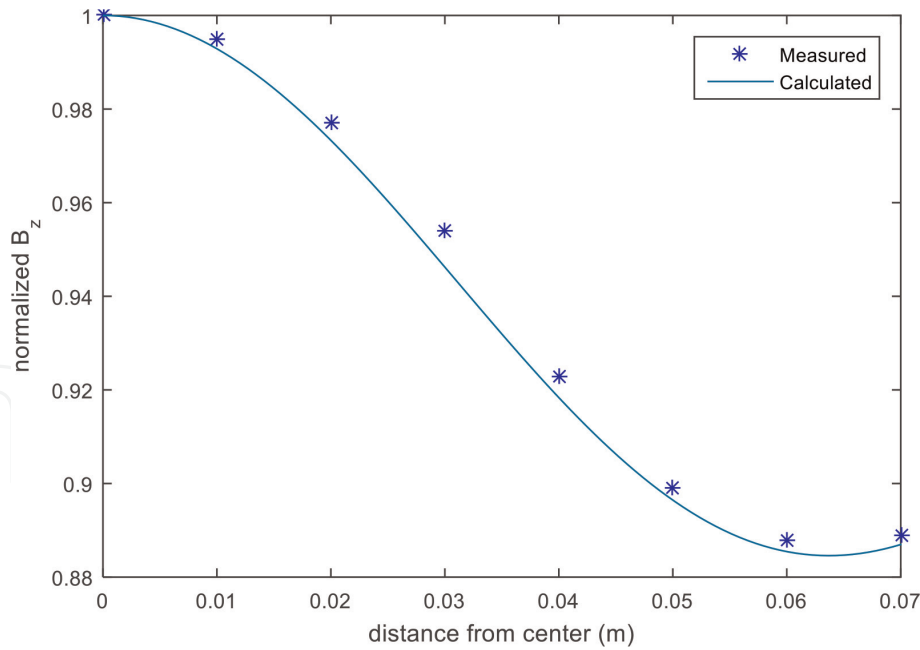


Figure 23.

Comparison of measured and calculated vertical magnetic field over the prototype mat.

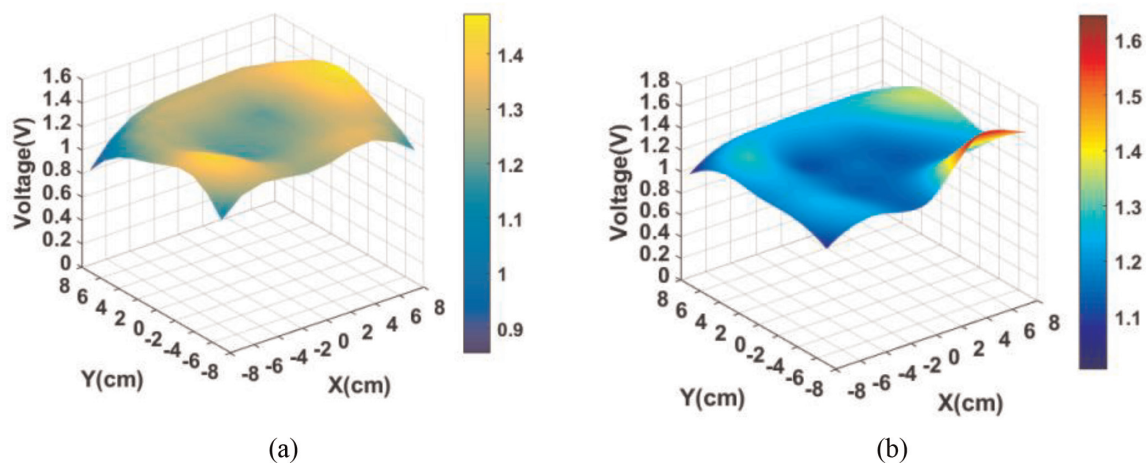


Figure 24.

Voltage distribution computed by interpolating the 21 measured voltage values across the load coil at a constant primary and secondary coil separation of (a) 8 cm and (b) 10 cm.

1.23 and 0.11 V, respectively. The relatively small standard deviation indicates a nearly uniform magnetic field distribution, as observed in **Figure 24**. The results indicate that a flat magnetic field can be achieved by our power mat design and that this design is effective for WPT to biomedical implants in freely moving animals.

4. Conclusion

We have presented a DH coil as the WPT receiver in implantable medical devices. This new coil has several attractive properties that it can be made conveniently at high precision on a flexible PCB along with other electronic components, forming a complete flexible sheet. This sheet, after being hermetically sealed, can be wrapped around a tubular biological structure, such as a blood vessel or a nerve bundle, to perform diagnostic, monitoring and therapeutic functions. The DH coil has been mathematically analyzed, and expressions for both mutual inductance and self-inductance have been derived. We have found that the DH coil provides a

higher coupling factor than the conventional solenoid coil when a lateral or angular misalignment exists. In addition, the DH coil achieves the largest coupling factor and energy transfer efficiency when the axis of the DH coil is in parallel with the plane of the planar spiral transmitter coil. Our computer simulation and experiments under lateral and angular misalignments have been conducted and their results have verified our analytical results.

In order to support biomedical studies using the animal model, we have designed a new power mat, enabling wireless power delivery to miniaturized moving targets. The power mat contains a single or multiple transmitter cells and each cell consists of seven hexagonally packed PSCs. We have conducted theoretical, computational and experimental studies on the special WPT system to meet the challenge of distributing the electromagnetic field evenly over the power mat. We have analyzed the HPT cell using the CMT. Formulas have been derived relating the received power to the inputs and system parameters. Then, we utilize computer simulation to study the evenness of the magnetic field distribution over the power mat at different distances between the power mat and the floor of the animal cage. Finally, we constructed a prototype system, measured its magnetic field distribution and verified that our design has met the challenge. We have also presented a new design of the receiver coil consisting of three serially connected sub-coils. This new design of the receiver coil allows it to capture the most magnetic flux produced by the transmitter, facilitates a match of resonant frequencies of the transmitter and receiver, and reduces the volume of the implant.

Author details

Qi Xu^{1,4}, Tianfeng Wang^{2,4}, Shitong Mao³, Wenyan Jia³, Zhi-Hong Mao^{3,5}
and Mingui Sun^{3,4,5*}

1 School of Artificial Intelligence and Automation, Huazhong University of Science and Technology, Wuhan, China

2 Department of Electrical Engineering, Shanghai Jiao Tong University, Shanghai, China


3 Department of Electrical and Computer Engineering, University of Pittsburgh, Pittsburgh, USA

4 Department of Neurosurgery, University of Pittsburgh, Pittsburgh, USA

5 Department of Bioengineering, University of Pittsburgh, Pittsburgh, USA

*Address all correspondence to: drsun@pitt.edu

IntechOpen

© 2019 The Author(s). Licensee IntechOpen. This chapter is distributed under the terms of the Creative Commons Attribution License (<http://creativecommons.org/licenses/by/3.0/>), which permits unrestricted use, distribution, and reproduction in any medium, provided the original work is properly cited. 

References

- [1] Ma A, Poon ASY. Midfield wireless power transfer for bioelectronics. *IEEE Circuits and Systems Magazine*. 2015; **15**(2):54-60. DOI: 10.1109/MCAS.2015.2418999
- [2] Jow U, Ghovanloo M. Design and optimization of printed spiral coils for efficient transcutaneous inductive power transmission. *IEEE Transactions on Biomedical Circuits and Systems*. 2007;**1**(3):193-202. DOI: 10.1109/TBCAS.2007.913130
- [3] RamRakhyani AK, Mirabbasi S, Mu C. Design and optimization of resonance-based efficient wireless power delivery systems for biomedical implants. *IEEE Transactions on Biomedical Circuits and Systems*. 2011; **5**(1):48-63. DOI: 10.1109/TBCAS.2010.2072782
- [4] Zhong WX, Zhang C, Xun L, Hui SYR. A methodology for making a three-coil wireless power transfer system more energy efficient than a two-coil counterpart for extended transfer distance. *IEEE Transactions on Power Electronics*. 2015;**30**(2):933-942. DOI: 10.1109/TPEL.2014.2312020
- [5] Zarifi T, Maunder A, Moez K, Mousavi P. Tunable open ended planar spiral coil for wireless power transmission. In: 2015 IEEE International Symposium on Antennas and Propagation & USNC/URSI National Radio Science Meeting, Canada; 19-24 July 2015
- [6] Seung Hee J, Zhigang W. Stretchable wireless power transfer with a liquid alloy coil. In: 28th IEEE International Conference on Micro Electro Mechanical Systems (MEMS); 18-22 January 2015; Portugal; 2015
- [7] Hasan N, Yilmaz T, Zane R, Pantic Z. Multi-objective particle swarm optimization applied to the design of wireless power transfer systems. In: *Wireless Power Transfer Conference (WPTC)*; USA: IEEE; 2015. 13-15 May 2015
- [8] Yakovlev A, Kim S, Poon A. Implantable biomedical devices: Wireless powering and communication. *IEEE Communications Magazine*. 2012; **50**(4):152-159. DOI: 10.1109/MCOM.2012.6178849
- [9] Ho JS, Yeh AJ, Neofytou E, Kim S, Tanabe Y, Patlolla B, et al. Wireless power transfer to deep-tissue microimplants. *Proceedings of the National Academy of Sciences*. 2014; **111**(22):7974-7979. DOI: 10.1073/pnas.1403002111
- [10] Available from: <http://www.implantable-device.com/category/technologies/wireless-power-transmission/>
- [11] Available from: <http://news.bostonscientific.com/news-releases?item=58598>
- [12] Ahn D, Ghovanloo M. Optimal design of wireless power transmission links for millimeter-sized biomedical implants. *IEEE Transactions on Biomedical Circuits and Systems*. 2016; **10**(1):125-137. DOI: 10.1109/TBCAS.2014.2370794
- [13] Kyungmin N, Heedon J, Hyunggun M, Bien F. Tracking optimal efficiency of magnetic resonance wireless power transfer system for biomedical capsule endoscopy. *IEEE Transactions on Microwave Theory and Techniques*. 2015;**63**(1):295-304. DOI: 10.1109/TMTT.2014.2365475
- [14] Loeb GE, Richmond FJ, Baker LL. The BION devices: Injectible interfaces with peripheral nerves and muscles. *Neurosurgical Focus*. 2006;**20**(5):1-9. DOI: 10.3171/foc.2006.20.5.3

- [15] Kimchi T, Xu J, Dulac C. A functional circuit underlying male sexual behaviour in the female mouse brain. *Nature*. 2007;**448**:1009-1014
- [16] Xu Q, Hu D, Duan B, He J. A fully implantable stimulator with wireless power and data transmission for experimental investigation of epidural spinal cord stimulation. *IEEE Transactions on Neural Systems and Rehabilitation Engineering*. 2015;**23**(4): 683-692. DOI: 10.1109/TNSRE.2015.2396574
- [17] OpenStax College. *Anatomy and Physiology*. Rice University, Houston: OpenStax College; 2013
- [18] Mao S, Wang H, Mao ZH, Sun M. A miniature implantable coil that can be wrapped around a tubular organ within the human body. *AIP Advances*. 2018;**8**(5):056629. DOI: 10.1063/1.5007258
- [19] Mao S, Wang H, Mao ZH, Sun M. A double-helix and cross-patterned solenoid used as a wirelessly powered receiver for medical implants. *AIP Advances*. 2018;**8**(5):056603. DOI: 10.1063/1.5007236
- [20] Yin N, Xu G, Yang Q, Zhao J, Yang X, Jin J, et al. Analysis of wireless energy transmission for implantable device based on coupled magnetic resonance. *IEEE Transactions on Magnetics*. 2012;**48**(2):723-726. DOI: 10.1109/TMAG.2011.2174341
- [21] Mayordomo I, Dräger T, Spies P, Bernhard J, Pflaum A. An overview of technical challenges and advances of inductive wireless power transmission. *Proceedings of the IEEE*. 2013;**101**(6): 1302-1311. DOI: 10.1109/JPROC.2013.2243691
- [22] Kurs A, Karalis A, Moffatt R, Joannopoulos JD, Fisher P, Soljacic M. Wireless power transfer via strongly coupled magnetic resonances. *Science*. 2007;**317**(5834):83-86. DOI: 10.1126/science.1143254
- [23] Xu Q, Wang H, Gao Z, Mao Z, He J, Sun M. A novel mat-based system for position-varying wireless power transfer to biomedical implants. *IEEE Transactions on Magnetics*. 2013;**49**(8): 4774-4779. DOI: 10.1109/TMAG.2013.2245335
- [24] Xu Q, Gao Z, Wang H, He J, Mao Z, Sun M. Batteries not included: A mat-based wireless power transfer system for implantable medical devices as a moving target. *IEEE Microwave Magazine*. 2013;**14**(2):63-72. DOI: 10.1109/MMM.2012.2234640
- [25] Graham RL, Lubachevsky BD, Nurmela KJ, Östergård PRJ. Dense packings of congruent circles in a circle. *Discrete Mathematics*. 1998;**181**(1-3): 139-154. DOI: 10.1016/S0012-365X(97)00050-2
- [26] Zhang F, Hackworth SA, Fu W, Li C, Mao Z, Sun M. Relay effect of wireless power transfer using strongly coupled magnetic resonances. *IEEE Transactions on Magnetics*. 2011;**47**(5): 1478-1481. DOI: 10.1109/TMAG.2010.2087010
- [27] Zhang F, Liu J, Mao Z, Sun M. Mid-range wireless power transfer and its application to body sensor networks. *Open Journal of Applied Sciences*. 2012;**2**(1):35-46. DOI: 10.4236/ojapps.2012.21004
- [28] Simpson J, Lane J, Immer J, Youngquist R. Simple analytic expressions for the magnetic field of a circular current loop. *NASA Technical Document Collection*. Document ID: 20010038494; 2001